
Proceedings Paper:
Kazemi, E., Tait, S., Shao, S. et al. (1 more author) (2016) Potential application of mesh-free SPH method in turbulent river flows. In: Rowiński, P. and Marion, A., (eds.) Hydrodynamic and Mass Transport at Freshwater Aquatic Interfaces. 34th International School of Hydraulics, May 2015, Zelechów, Poland. Springer Verlag , pp. 11-22.

https://doi.org/10.1007/978-3-319-27750-9_2

Potential application of mesh-free SPH method in turbulent river flows

Ehsan Kazemi, Simon Tait, Songdong Shao and Andrew Nichols

Abstract A comprehensive review has been completed on the simulation of turbulent flow over rough beds using mesh-free particle models. Based on the outcomes of this review an improved Smoothed Particle Hydrodynamics (SPH) method has been developed for open channel flows over a rough bed, in which a mixing length model is used for modeling the 2D turbulence and a drag force equation is proposed for treating the boundary shear. The proposed model was applied to simulate a depth-limited open channel flow over a rough bed surface. The results of the velocity profile and shear stress distribution show a good agreement with the experimental data and existing analytical solutions. This work reveals that in order to correctly model turbulent open channel flow over a rough bed, the treatment of both flow turbulence and bed roughness effect is equally important.

1. Introduction

Turbulence behavior in natural river flow is one of the most important issues in river engineering as it can generate a significant effect on the flow structure and plays a key role in the transport of sediments especially fine suspended particles. Since river flows are usually turbulent and the river beds are often composed of sands, gravels, ripples, or dunes, the study of turbulent flow over rough bed channels has been an important topic in the last decades. However, the flow behavior near the bed and the effect of rough elements on the flow velocity and turbulence characteristics are not fully understood yet.

The main effect of bed roughness is on the vertical distribution of flow velocity and turbulence near the bed, which then affects the whole flow structure. As the roughness characteristics and bed geometry vary from one river channel to another, the effects of roughness on the flow are different and should be treated differently in various theoretical and numerical studies. However, most of models for sand grain bed roughness have assumed a standard organized roughness pattern and so related the roughness effect with an equivalent roughness height. The classical scheme based on experimental data of Nikuradse [23], Clauser [3], Rotta [26] and Perry et al. [24] revealed that the flow velocity profile in a semi-logarithmic

E. Kazemi · S. Tait · S. Shao (✉) · A. Nichols
Department of Civil and Structural Engineering, University of Sheffield, Sheffield S1 3JD, UK
e-mail: s.shao@sheffield.ac.uk

scale has the same slope (von-Karman constant, κ) for both the smooth and rough walls, but with a vertical shift in the mean velocity for the case of a rough wall. A number of research studies have been carried out to find a relationship between the shift in velocity and the physical roughness size and also to find the effective location of the wall, i.e. where the flow mean velocity is zero. Based on the experiments for uniform sand grain roughness, Nikuradse [23] found that the shift is a function of the equivalent roughness height $k_s^+ = k_s u^*/\nu$ only, where k_s is the diameter of the sand grain, u^* is the boundary shear velocity, ν is the kinematic viscosity and vertical coordinate z is measured from some distance below the top of the sand grain. However, the data analysis made by Clauser [3] has shown that the shift is also related to the pattern and shape of the roughness. Generally speaking, the effect of bed roughness on the velocity field and flow turbulence has not been precisely addressed because of the complex nature of this problem. On the other hand, numerous experimental and numerical studies have been carried out to understand the complicated process of turbulent channel flows and their interactions with the bed. With regard to the treatment of rough bed surfaces, Table 1 summarizes some existing numerical models as well as an assessment of their strengths and weaknesses.

Table 1. Summary of numerical models treating shear boundary layer near rough wall

Boundary treatment method	Turbulence model	Characteristics	Examples
Wall function model	k-ε model	Suitable for smooth and small-scale boundary roughness, but not efficient for large-scale one as the velocity distribution is not logarithmic near rough wall	Hsu et al. [12], Nicholas and Smith [21], Zeng and Li [34]
Modified turbulence model	Mixing length model	Simple but applicable only for shear flows where the distribution of the mixing length is known	van Driest [30], Rotta [26], Granville [10,11], Krogstad [13]
Drag-force model	Any turbulence model	Suitable for rough boundaries with large discrete roughness elements, also reflects the effects of rough wall based on shape and geometry of the roughness element	Christoph and Pletcher [2], Taylor et al. [29], Wiberg and Smith [33], Miyake et al. [17], Cui et al. [4], Rameshwaran et al. [25], Zeng and Li [34]

2. Mesh-free particle models for open channel flow

In recent years, mesh-free particle modelling approaches, such as SPH, have been investigated for their potential in simulating open channel flows, but their poten-

tial has not been fully explored for the turbulent channel flows over rough wall boundaries. There are two main reasons for this, firstly the lack of adequate turbulence models which can be used to close with the Lagrangian SPH equations, and secondly the difficulty in modelling the flow structure near wall boundaries especially when the wall is composed of rough elements. In the following section, established turbulence and rough bed models used in existing particle based methods are reviewed.

2.1. Turbulence modelling in particle methods

Turbulence modelling in particle methods is very challenging as all well-known turbulence models have been originally developed and tested for the mesh-based methods. However, there have been some attempts in recent years to apply different turbulence models in particle methods. One of the earliest and successful works was made by Gotoh et al. [9] who applied a sub-particle scale (SPS) turbulence model in their Moving Particle Semi-implicit (MPS) method for simulating a turbulent jet. The key idea of this approach is that large scale turbulent eddies are resolved by the spatially averaged Navier-Stokes (N-S) equations and small scale eddies are calculated through the SPS formulation which relates the Reynolds stress to the mean flow strain rate according to the Boussinesq approximation. Later on, Violeau et al. [32] proposed two approaches in modelling the flow turbulence in SPH. One was based on the eddy viscosity assumption and another was based on the Generalized Langevin Model (GLM). They tested these two turbulence models by solving the Lagrangian form of N-S equations for a turbulent Poiseuille flow in a pipe. Violeau and Issa [31] also developed turbulence models to be used with SPH for some complex free surface flows. They developed a k-ε model as well as an explicit algebraic Reynolds stress model (EARSM) and they even used a 3D Large Eddy Simulation (LES) model to simulate the collapse of a water column. The authors stated that, despite of its simplicity, the LES-SPS model needs more computational costs in comparison with the traditional RANS turbulence closures. Lopez et al. [14] developed a SPH model for the hydraulic jumps with different Froude numbers (Fr). They achieved good result for the cases with low Froude number by using the standard SPH formulations without any turbulence closure, but a variable artificial viscosity formulation had to be used to achieve good accuracy for flows with $Fr > 5$. In addition, some researchers have applied Smagorinsky-based SPS models in turbulence modelling for the particle methods, including but not limited to Sahebari et al. [27], Chern and Syamsuri [1] and Fu and Jin [7], where the Smagorinsky constant was taken 0.12 to 0.15 in their models. In a recent study, De Padova et al. [5] used a mixing length model for 3D hydraulic jumps in a large channel. The turbulence model was first validated by simulating a 2D uniform open channel flow over a wall with roughness size k_s = 0.02H, where H is the water depth. Then it was used to simulate hydraulic jumps

and the model result of free surface profiles was compared with that computed by a k-ε model.

2.2. Rough bed boundary treatment in particle methods

In addition to the inclusion of turbulence model, the treatment of bed boundary is also very important in modelling open channel flows. However, in most of the developed particle models, the effect of bed roughness is not taken into consideration. Shakibaeinia and Jin [28], Sahebari et al. [27], Federico et al. [6] and De Padova et al. [5] have not explicitly included any treatment of the channel bed in their models. On the other hand, this issue has been tentatively addressed in some other mesh-free SPH and MPS models. Violeau et al. [32] and Violeau and Issa [31] applied a wall function approach to their turbulence models to impose the logarithmic velocity distribution near the wall. Lopez et al. [14] applied a Lennard-Jones repulsive force on the bed to prevent the particles from penetrating into the wall and this produced a "numerical" resistance arising from the roughness effect. Chern and Syamsuri [1] used bottom boundaries for the smooth, triangular, trapezoidal and sinusoidal beds defined by lines of particles to simulate the effect of corrugated bed on the hydraulic jump characteristics. They used a repulsive force similar to Lopez et al. [14] in that the wall particles exert a force on the fluid particles to represent the resistance of the rough bed. Fu and Jin [7] accounted for the bed roughness in their MPS model by setting several layers of ghost particles beyond the bed boundary and assigning an artificial velocity to these imaginary particles in the opposite direction of the flow. The model presented a simple method to reflect the effect of bottom roughness on the flow by imposing a numerical adjustment of velocity at the bed, which was not based on an actual physical mechanism.

As reviewed, in most of mesh-free particle models developed for open channel flows, bed roughness effect is not explicitly accounted for. Since the bed is the main source of turbulence production, there should be some treatments in the numerical modelling for the flow over rough surfaces. The roughness reduces velocity near the bed to produce a velocity gradient, and this effect can be transferred to the upper layers of the flow by the turbulent shear stress. According to the summary presented in Table 1, the drag force method coupled with a suitable turbulence model has been shown to be an appropriate way of modelling the roughness effect in grid-based methods [29, 33, 34], which can be also applied in mesh-free particle methods. Ideally, the production of near-wall velocity gradient can be modelled by an appropriate drag force model and the transportation of shear to upper layers can be modelled by a suitable turbulence model.

Thus the aim of the present study is to investigate the feasibility of mesh-free particle methods (e.g. SPH) and propose effective solutions for the simulation of turbulent open channel flows over a rough bed surface. We suggest applying a drag

force equation to account for the effect of bed roughness based on the selection of drag force models as found in the literature, and coupling it with a suitable mixing length model to address the flow turbulence effect. The mixing length approach is preferred because of its simplicity and effectiveness in modelling shear flows.

3. SPH model and its application

In this application study, a numerical model is developed by the authors based on the SPH method to solve the 2D Lagrangian form of conservation equations of mass and momentum to simulate a depth-limited turbulent open channel flow over a fully rough bed consisting of regular spheres. This model is developed to ultimately provide a mesh free based modelling capability to simulate the flow over and within rough, potentially mobile porous boundaries. The development is part of the EU funded HYTECH project that is focusing on the physical processes at important aquatic boundaries [16]. The solved equations of the current version of the model are defined as

$$\frac{\mathrm{D}\rho}{\mathrm{D}t} = -\rho\nabla\cdot\mathbf{u} \tag{1}$$

$$\frac{\mathrm{D}\mathbf{u}}{\mathrm{D}t} = -\frac{1}{\rho}\nabla \mathrm{P} + \mathbf{g} + \nu_0\nabla^2\mathbf{u} + \frac{1}{\rho}\nabla\cdot\boldsymbol{\tau} + \frac{1}{\rho}\boldsymbol{\tau}_{\mathrm{d}} \tag{2}$$

where t (s) is time, ρ (kg/m^3) is density, $\mathbf{u}$ (m/s) is velocity, P (Pa) is pressure, $\mathbf{g}$ (m/s^2) is gravitational acceleration, v_0 (m^2/s) is kinematic viscosity of water, $\boldsymbol{\tau}$ (Pa) is turbulent shear stress tensor and $\boldsymbol{\tau}_d$ (Pa/m) is drag-induced shear stress. The fourth term on the right hand side of the momentum equation can be modelled by using different turbulence closure models. In a 2D uniform open channel flow, by considering x and z as horizontal and vertical coordinates respectively, $\nabla\cdot\boldsymbol{\tau}$ can be simply substituted by $\partial\tau_{xz}/\partial z$, where τ_{xz} is the xz component of the shear stress tensor, since other stress components are much smaller and can thus be ignored. According to the mixing length theory, the following equation can be solved for the turbulent shear stress

$$\frac{\tau_{\mathrm{xz}}}{\rho} = \mathrm{l_m}^2\left|\frac{\partial \mathrm{u}}{\partial \mathrm{z}}\right|\left(\frac{\partial \mathrm{u}}{\partial \mathrm{z}}\right) \tag{3}$$

where u (m/s) is the velocity component in x direction and l_m (m) is the mixing length which is calculated by Nezu and Rodi formula [20].

The fifth term on the right hand side of the momentum equation is the drag stress term added to account for the effect of rough bed boundary. This term is calculat-

ed only for the particles which are located in a namely drag zone (see Fig. 1), where the drag-induced shear stress $\boldsymbol{\tau}_d$ is calculated by the following equation

$$\boldsymbol{\tau}_{\mathrm{d}} = \frac{\mathbf{F}_{\mathrm{d}}}{\mathrm{A}_{\tau}} \tag{4}$$

where $\mathbf{F}_d$ (N) is the drag force exerted on fluid particle from the bed, which is assumed to be equal to and in the opposite direction of the force from the fluid particle to the bed, and A_τ (m^2) is the bed-parallel planar area affected by the fluid particle which is equal to $d_s d_p$ (where d_s is the bed grain diameter and d_p is the SPH particle spacing). The drag force $\mathbf{F}_d$ is calculated by

$$\mathbf{F}_{\mathrm{d}} = -\frac{1}{2}\mathrm{C}_{\mathrm{d}}\rho\mathrm{A}_{\mathrm{d}}\mathbf{u}|\mathbf{u}| \tag{5}$$

where C_d is the drag coefficient and A_d (m) is the cross-sectional area that is equal to the particle spacing d_p.

As mentioned before, the SPH method is used to discretize the governing equations. SPH is a Lagrangian particle approach that was developed by Gingold and Monaghan [8] and Lucy [15] initially for the astrophysical problems. Then it was used widely for simulating the fluid flows. In the SPH approximation, a variable like "A" is estimated at the location of particle "a" according to the values at neighboring particles "b" by the following equation

$$\mathrm{A}(\mathbf{r}_{\mathrm{a}}) = \sum_{\mathrm{b}} \mathrm{m}_{\mathrm{b}} \frac{\mathrm{A}(\mathbf{r}_{\mathrm{b}})}{\rho_{\mathrm{b}}} \mathrm{W}(\mathbf{r}_{\mathrm{a}} - \mathbf{r}_{\mathrm{b}}, \mathrm{h}) \tag{6}$$

where $\mathbf{r}$ is the particle position, h is the smoothing length, m_b and ρ_b are respectively the mass and density of neighboring particles, and $W(\mathbf{r}_a\text{-}\mathbf{r}_b,h)$ is the weighting or kernel function that is specified by a cubic spline function in the present work (refer to [19]). The derivative of $A(\mathbf{r}_a)$ in x_j direction can be approximated as follows

$$\frac{\partial \mathrm{A}(\mathbf{r}_{\mathrm{a}})}{\partial \mathrm{x}_{\mathrm{j}}} = \sum_{\mathrm{b}} \mathrm{m}_{\mathrm{b}} \frac{\mathrm{A}(\mathbf{r}_{\mathrm{b}})}{\rho_{\mathrm{b}}} \frac{\partial \mathrm{W}(\mathbf{r}_{\mathrm{a}} - \mathbf{r}_{\mathrm{b}}, \mathrm{h})}{\partial \mathrm{x}_{\mathrm{j}}} \tag{7}$$

According to the SPH formulations, the governing equations (1 and 2) are discretized as below respectively to calculate the density and velocity of particles

$$\frac{\mathrm{D}\rho_{\mathrm{a}}}{\mathrm{Dt}} = \rho_{\mathrm{a}} \sum_{\mathrm{b}} \frac{\mathrm{m}_{\mathrm{b}}}{\rho_{\mathrm{b}}} \mathbf{u}_{\mathrm{ab}} \cdot \nabla_{\mathrm{a}} \mathrm{W}_{\mathrm{ab}} \tag{8}$$

$$\begin{aligned}\frac{d\mathbf{u}_a}{dt} &= -\sum_b m_b\left(\frac{P_a}{\rho_a^{\,2}}+\frac{P_b}{\rho_b^{\,2}}\right)\nabla_a W_{ab}+\mathbf{g}\\ &+\sum_b m_b\frac{4\nu_0}{(\rho_a+\rho_b)}\frac{\mathbf{r}_{ab}\cdot\nabla_a W_{ab}}{|\mathbf{r}_{ab}|^2+\eta^2}\mathbf{u}_{ab}\\ &+\sum_b m_b\left(\frac{\boldsymbol{\tau}_a}{\rho_a^{\,2}}+\frac{\boldsymbol{\tau}_b}{\rho_b^{\,2}}\right)\cdot\nabla_a W_{ab}+\frac{1}{\rho_a}(\boldsymbol{\tau}_d)_a\end{aligned} \tag{9}$$

where $\mathbf{u}_{ab} = \mathbf{u}_a - \mathbf{u}_b$, $\mathbf{r}_{ab} = \mathbf{r}_a - \mathbf{r}_b$, $\nabla_a W_{ab}$ is the gradient of the kernel function between particles "*a*" and "*b*" with respect to the position of particle "*a*", and η is a small number introduced to avoid a zero denominator during computations and is set to $0.1h$. In the present model, the following equation is used to relate the pressure explicitly with the fluid density as

$$P = c_0^{\,2}(\rho-\rho_0) \tag{10}$$

where ρ_0 is the reference density and c_0 is the speed of sound. In SPH, it is assumed that the flow is slightly compressible so the speed of sound is chosen to be much smaller than the physical one to ensure the fluid compressibility being less than 1%. ρ_0 and c_0 are thus taken 1000 (kg/m^2) and 16 (m/s) respectively in the present study. To solve the equations in time, a predictor-corrector marching scheme is applied (refer to [18]).

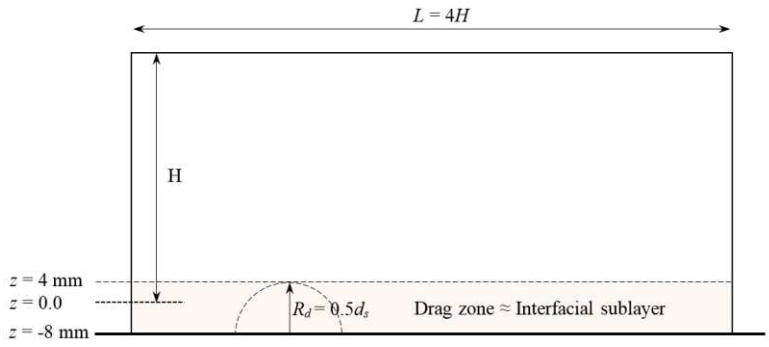

Fig. 1. A schematic view of the computational domain and drag zone

To assess the capability of the proposed SPH model, a test case of open channel flow over a rough bed is simulated and the model results are validated by comparing with experimental data. In the experimental tests, a steady uniform flow with water depth H = 50 mm was established in a 0.459 m wide and 12 m long laboratory flume with a gradient of S_0 = 0.004 [22]. The bed was composed of hexagonally packed spheres with a diameter d_s = 24 mm. Two-dimensional Particle Image Velocimetry (PIV) was used to measure the time-dependent flow field beneath

the water surface, in a vertical plane along the centerline of the flume at a position of 8.4 m from the flume inlet. Two calibrated CCD cameras with an image area of 1600 x 600 pixels, were focused on the laser sheet, and were synchronized with the laser pulses. The overlapping field of view of these two cameras covered an area of approximately 247 mm x 89 mm. Neutrally buoyant PIV seeding particles were added to the flow and a pair of particle images separated by a time delay of 1 ms was captured on each camera. This was repeated at a fixed frequency of 26.9 Hz for a duration of 5 minutes.

Each image pair from the two PIV cameras was divided into interrogation areas with a physical area of around 4.9 x 4.9 mm, with a 50 % overlap so that the spatial resolution of the measurements was around 2.5 mm. A two dimensional cross-correlation technique determined the velocity vector for each interrogation area by comparing the images captured in the frame pairs. Vector maps then underwent range validation and moving average validation to correct any spurious data points, with fewer than 5% of vectors being replaced. Finally, the vector maps from the two PIV cameras were combined to form a time series of vector maps which would enable comparison with the SPH data.

Since the bed elements have a diameter d_s = 24 mm, half of d_s is taken as the effective roughness height (R_d) in the model. The drag stress term is calculated only for the particles located within a distance less than $R_d = d_s/2$ from the bed. A sketch view of the computational domain is shown in Fig. 1. There are different values of drag coefficient C_d as addressed in the literature for spheres. This coefficient is set equal to 0.5 in the present study for universality at high Reynolds Numbers. The initial SPH particle spacing is 2 mm. As shown in Fig. 1, the zero datum in the model is set 4 mm below the top of the sphere for consistency with the experimental data, and the bed level which is $d_s/2$ below the top of the sphere is located at z = -8 mm. The relevant computational parameters are summarized in Table 2.

Table 2. Computational parameters

H (mm)	S_0	d_s (mm)	C_d	R_d (mm)	d_p (mm)
50	0.004	24	0.5	12	2

Fig. 2a shows the comparison between time-averaged computed and measured streamwise velocity profiles. It can be seen that there is good agreement with the experimental data in terms of magnitude and slope of the velocity profile. According to Fig. 2b, the SPH model can also accurately predict the shear stress close to the analytical solutions ($\tau = \rho g S_0 (1 - z/H)$). Meanwhile, Fig. 2c shows the distribution of the drag stress term (τ_d/ρ) in streamwise (x) direction. As shown in Fig. 2b, the maximum turbulent shear stress occurs at the top of the bed grain. This is because the velocity gradient is a maximum at this interface due to the drag force effect. The simulation results have revealed that the mixing length model coupled

with the drag force equation worked well in estimating the roughness effect on the flow. The drag force produced an extra shear stress near the bed and the mixing length model transported the resulting effect through the water depth.

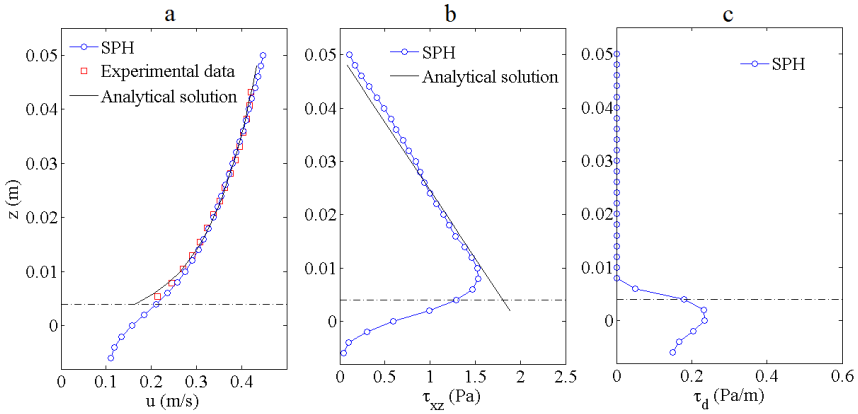

Fig. 2. Results of the model: a) streamwise velocity; b) turbulent shear stress; c) drag-induced stress term. The dash-dotted line shows top level of the bed particles.

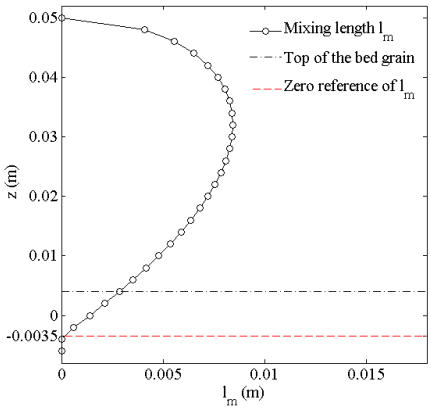

Fig. 3. Vertical distribution of the calculated mixing length.

Fig. 3 shows the distribution of mixing length calculated by Nezu and Rodi formula [20]. According to this, l_m increases from zero at the reference datum below the top of the bed grain with a slope $\kappa = 0.41$ (according to Prandtl's theory) and then decreases to zero at the free surface. According to Nezu and Rodi [20], this decrease is due to the fact that the water surface restricts the size of turbulence eddies and hence reduces the turbulent length scale. In this study, the zero-reference of the mixing length profile is set at z = -3.5 mm, i.e. 4.5 mm above the bed level (See Fig. 3) and below this level l_m is assumed to be zero. However, in some other studies, the distribution of mixing length in the interfacial sub-layer is assumed in a different way (For instance see [34]). In the present work, the zero-reference of

the mixing length has been found by using numerical trials so as to achieve the best fit of mean velocity profile to the measured data.

To further investigate the importance of the turbulence model, the calculations have been repeated by applying the SPS model (Gotoh et al. [9]) with the Smagorinsky constant $C_s = 0.15$ and a filter size (Δ) equal to the SPH particle spacing d_p. Here, the product of $C_s\Delta$ should be equivalent to the mixing length l_m, but it remains constant with a value of 0.0003. Comparing this value with the mixing length value obtained in the previous simulation as shown in Fig. 3, the turbulent shear stress will be expected to be underestimated. This is demonstrated in Fig. 4b, where the turbulent shear stress calculated by the SPS-Smagorinsky model is compared with the analytical solution and the shear stress calculated by the mixing length model. Fig. 4a also presents a comparison between the SPS-Smagorinsky model, SPH-mixing length model, experimental data and the analytical solution in terms of time-averaged streamwise velocity. Due to the underestimation of the turbulent shear stress, the velocity profile is not correctly reproduced by the SPS-Smagorinsky model. Thus it can be noticed that the SPS model with $C_s = 0.15$ is unable to predict the correct mechanism of momentum transfer in 2D uniform turbulent channel flow over a rough bed. Nonetheless, this model might be successfully applied to non-uniform or 3D open channel flows, where the shear strains are significant in the two other directions (see [31]).

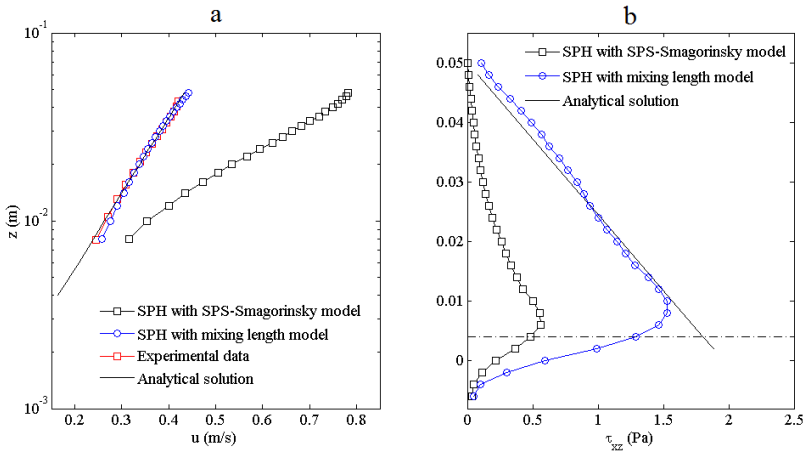

Fig. 4. Comparison of results between the mixing length model and the SPS-Smagorinsky model with $C_s = 0.15$. a) Semi-logarithmic streamwise velocity; b) Turbulent shear stress. The dash-dotted line shows top level of the bed grain.

4. Conclusions

In this paper, a comprehensive review has been completed on turbulence models and shear boundary layer treatment used in existing particle models in order to

find potential applicability of the SPH method in modelling open channel flows over rough bed boundaries. Accordingly, the mixing length model has been suggested for turbulence modelling and the drag-induced shear stress has been proposed to be included in the N-S equations to account for the roughness effect. A numerical model has been developed based on the SPH method coupled with the proposed approaches and finally a test case of turbulent open channel flow over a fully rough channel bed has been solved by the developed model. The numerical results were compared to experimental data and analytical solutions where a good agreement was observed in terms of flow velocity and shear stress. This indicated that the drag force model successfully reproduced the mechanism of velocity reduction in the shear boundary layer and the mixing length model correctly transferred this effect to the upper flow. It has also been shown that the SPS-Smagorinsky model with $C_s = 0.15$ was unable to reproduce the correct turbulent shear stress in uniform open channel flows over rough beds. Hence, for modelling such flows, the SPS-Smagorinsky model could be adopted but with a mixing length approach to determine the eddy viscosity, instead of using the fixed Smagorinsky constant.

Acknowledgements This work was supported by the Research Executive Agency, through the 7th Framework Programme of the European Union, Support for Training and Career Development of Researchers (Marie Curie - FP7-PEOPLE-2012-ITN), which funded the Initial Training Network (ITN) HYTECH 'Hydrodynamic Transport in Ecologically Critical Heterogeneous Interfaces', N.316546.

5. References

1. Chern M, Syamsuri S (2013) Effect of corrugated bed on hydraulic jump characteristic using SPH method. Journal of Hydraulic Engineering, 139(2):221–232.
2. Christoph GH, Pletcher RH (1983) Prediction of rough-wall skin friction and heat transfer. AIAA Journal, 21:509–515.
3. Clauser FH (1954) Turbulent boundary layers in adverse pressure gradients. Journal of Aeronautical science, 21:91–108.
4. Cui J, Patel VC, Lin CL (2003) Prediction of turbulent flow over rough surfaces using a force field in large eddy simulation. Journal of Fluids Engineering, Trans ASME, 125:2–9.
5. De Padova D, Mossa M, Sibilla S, Torti E (2013) 3D SPH modelling of hydraulic jump in a very large channel. Journal of Hydraulic Research, 51(2):158-173.
6. Federico I, Marrone S, Colagrossi A, Aristodemo F, Antuono M (2012) Simulating 2D open-channel flows through an SPH model. European Journal of Mechanics B/Fluids, 34:35–46.
7. Fu L, Jin YC (2013) A mesh-free method boundary condition technique in open channel flow simulation. Journal of Hydraulic Research, 51(2):174-185.
8. Gingold RA, Monaghan JJ (1977). Smoothed particle hydrodynamics: theory and application to non-spherical stars. Monthly Notices of the Royal Astronomical Society, 181:375--398.
9. Gotoh H, Shibahara T, Sakai T (2001) Sub-particle-scale turbulence model for the MPS method—Lagrangian flow model for hydraulic engineering. Computational Fluid Dynamics Journal, 9(4):339–347.
10. Granville PS (1985) Mixing-length formulations for turbulent boundary layers over arbitrary rough surfaces. Journal of Ship Research, 29(4):223–233.

11. Granville PS (1988) Eddy viscosities and mixing lengths for turbulent boundary layers on flat plates, smooth or rough. Journal of Ship Research, 32:229–237.
12. Hsu CC, Wu FS, Lee WJ (1998) Flow at 90 degrees equal-width open-channel junction. Journal of Hydraulic Engineering, ASCE, 124:186–91.
13. Krogstad PA (1991) Modification of the van driest damping function to include the effects of surface roughness. AIAA Journal, 29:888–894.
14. Lopez D, Marivela R,Garrote L (2010) Smoothed particle hydrodynamics model applied to hydraulic structures: a hydraulic jump test case. Journal of Hydraulic Research, 48:142-158.
15. Lucy LB (1977) Numerical approach to testing the fission hypothesis. Astronomical Journal, 82(12):1013–1024.
16. Marion A, Nikora V, Puijalon S, Bouma T, Koll K, Ballio F, Tait S, Zaramella M, Sukhodolov A, O'Hare M, Wharton G, Aberle J, Tregnaghi M, Davies P, Nepf H, Parker G & Statzner B (2014). Aquatic interfaces: a hydrodynamic and ecological perspective. Journal of Hydraulic Research, 52(6):744–758. DOI:10.1080/00221686.2014.968887.
17. Miyake Y, Tsujimoto K, Agata Y (1999) A DNS of a turbulent flow in a rough-wall channel using roughness elements model. JSME International Journal, 43(2):233-242.
18. Monaghan JJ (1989) On the problem of penetration in particle methods. Journal of Computational Physics, 82(1):1–15.
19. Monaghan JJ, Lattanzio JC (1985) A refined method for astrophysical problems. Astronomy and Astrophysics, 149:135–143.
20. Nezu I, Rodi W (1986) Open-channel flow measurements with a Laser Doppler anemometer. Journal of Hydraulic Engineering, ASCE, 112(5):335–355.
21. Nicholas AP, Smith GHS (1999). Numerical simulation of three-dimensional flow hydraulics in a braided channel. Hydrological Processes, 13:913–29.
22. Nichols A (2013) Free surface dynamics in shallow turbulent flows. PhD thesis, School of Engineering, University of Bradford, UK.
23. Nikuradse J (1933) Laws of flow in rough pipes. VDI Forschungsheft 361. English translation: NACA TM 1292, 1950.
24. Perry AE, Schofield WH, Joubert PN (1969). Rough wall turbulent boundary layers. Journal of fluid Mechanics, 37(2):383–413.
25. Rameshwaran P, Naden PS, Lawless M (2011) Flow modelling in gravel-bed rivers: rethinking the bottom boundary condition. Earth Surface Processes and Landforms, 36:1350–66.
26. Rotta J (1962) Turbulent Boundary layers in incompressible flow. Progress in Aerospace Science, Oxford, UK, 2:73–82.
27. Sahebari AJ, Jin YC, Shakibaeinia A (2011) Flow over sills by the MPS mesh-free particle method. Journal of Hydraulic Research, 49(5):649–656.
28. Shakibaeinia A, Jin YC (2011) MPS-based mesh-free particle method for modeling open-channel flows. Journal of Hydraulic Engineering, 137:1375–1385.
29. Taylor RP, Colemau HW, Hodge BK (1985) Prediction of turbulent rough-wall skin friction using a discrete element approach. ASME Journal of Fluids Engineering, 107:251–257.
30. van Driest ER (1956) On turbulent flow near a wall. Journal of Aeronautical Sciences, 23:1007–1011.
31. Violeau D, Issa R (2007) Numerical modelling of complex turbulent free-surface flows with the SPH method: an overview. International Journal for Numerical Methods in Fluids, 53(2):277–304.
32. Violeau D, Piccon S, Chabard JP (2002) Two attempts of turbulence modelling in smoothed particle hydrodynamics. Proceedings of the 8th Symposium on Flow Modelling and Turbulence Measurements. Advances in Fluid Modelling and Turbulence Measurements. World Scientific: Singapore, 339–346.
33. Wiberg PL, Smith JD (1991) Velocity distribution and bed roughness in high-gradient streams. Water Resources Research, 27:825–38.
34. Zeng C, Li CW (2012) Modeling flows over gravel beds by a drag force method and a modified S–A turbulence closure. Advances in Water Resources, 46:84–95.